

Identification of microplastics by FTIR and Raman microscopy: a novel silicon filter substrate opens the important spectral range below 1300 cm^{-1} for FTIR transmission measurements

Andrea Käppler^{1,2} · Frank Windrich^{2,3} · Martin G. J. Löder⁴ · Mikhail Malanin¹ · Dieter Fischer¹ · Matthias Labrenz⁵ · Klaus-Jochen Eichhorn¹ · Brigitte Voit^{1,2}

Received: 28 April 2015 / Revised: 10 June 2015 / Accepted: 11 June 2015 / Published online: 28 June 2015
© Springer-Verlag Berlin Heidelberg 2015

Abstract The presence of microplastics in aquatic ecosystems is a topical problem and leads to the need of appropriate and reliable analytical methods to distinctly identify and to quantify these particles in environmental samples. As an example transmission, Fourier transform infrared (FTIR) imaging can be used to analyze samples directly on filters without any visual presorting, when the environmental sample was afore extracted, purified, and filtered. However, this analytical approach is strongly restricted by the limited IR transparency of conventional filter materials. Within this study, we describe a novel silicon (Si) filter substrate produced by photolithographic microstructuring, which guarantees sufficient transparency for the broad mid-infrared region of $4000\text{--}600\text{ cm}^{-1}$. This filter type features holes with a diameter of $10\text{ }\mu\text{m}$ and exhibits adequate mechanical stability. Furthermore, it will be shown that our Si filter substrate allows a distinct identification of the most common microplastics, polyethylene (PE), and polypropylene (PP), in the characteristic fingerprint

region ($1400\text{--}600\text{ cm}^{-1}$). Moreover, using the Si filter substrate, a differentiation of microparticles of polyesters having quite similar chemical structure, like polyethylene terephthalate (PET) and polybutylene terephthalate (PBT), is now possible, which facilitates a visualization of their distribution within a microplastic sample by FTIR imaging. Finally, this Si filter can also be used as substrate for Raman microscopy—a second complementary spectroscopic technique—to identify microplastic samples.

Keywords Filter substrate · Microplastic identification · FTIR imaging · Raman · Silicon filter

Introduction

The presence of microplastics, i.e., micro-sized particles of synthetic polymers in a size range from 5 mm down to a few microns [1, 2], in marine ecosystems is documented for many different habitats worldwide. Microplastics were observed not only at the sea surface [3, 4], in the water column [5–7], and in beach sediments [8, 9] but also down to deep-sea sediments [10]. Furthermore, microplastics also affect limnic waters that are highly frequented by shipping or tourism, like rivers [11] and lakes [12, 13], but also remote waters face the problem of microplastic pollution [14]. Given the presence of microplastics in freshwater ecosystems, it is obvious that terrestrial ecosystems should be investigated with regard to the presence of microplastics and their biological effects [15].

In principle, microplastics can arise from all types of mismanaged plastic waste via UV degradation and mechanical abrasion [1]. These mainly fragmented particles as well as residues of washed out cloth fibers are counted among secondary microplastics. Together with so-called primary

✉ Andrea Käppler
kaeppler@ipfdd.de

¹ Leibniz Institute of Polymer Research Dresden, Hohe Str. 6,
01069 Dresden, Germany

² Organic Chemistry of Polymers, TU Dresden,
01062 Dresden, Germany

³ Fraunhofer Institute for Reliability and Microintegration - All Silicon
System Integration Dresden, Ringstraße 12,
01468 Moritzburg, Germany

⁴ Animal Ecology I, University of Bayreuth,
95440 Bayreuth, Germany

⁵ Leibniz Institute of Baltic Sea Research, Seestraße 15,
18119 Rostock, Germany

microplastics, which are produced as industrial raw pellets or as small-sized particles for the use in, e.g., cosmetic products [16–18] and washing and cleaning agents, a broad spectrum of differently shaped microplastics (fibers, fragmented particles, spherical granulates, etc.) can enter the environment.

Basically, microplastics in marine ecosystems can originate from two different sources, inland or offshore. Sea-based sources include waste and fragmented particles from fishing activities (nets, ropes) [1], shipping (tourism, merchant) [19], and offshore platforms [20], for instance. However, the main part of plastic debris in the oceans seems to originate from inland sources [1]. The input of land-based plastic debris into the marine environment was estimated to 4.8–12.7 million metric tons in 2010 [21]. The transport of land-based microplastics to the oceans is driven by rivers, sewage waters, or wind flow [20].

The biological impacts of microplastics on marine ecosystems and the involved working mechanisms are being intensively studied. Negative effects have been reported. Because of their small size, microplastics can be mistaken for food and can be ingested by a variety of organisms [22], ranging from filtering copepods [23, 24], over bivalves cultured for human consumption [25] to wildlife fishes [26, 27]. In addition to physical harm following ingestion of microplastics (intern and extern lesions, blockage of the intestinal tract) [28], their additives like endocrine-disrupting plasticizers or flame retardants as well as adsorbed and accumulated toxic contaminants like PCB and PAH [29, 30] pose a potential risk for the marine food web. Furthermore, microplastics are considered as a transport vehicle for potential pathogenic microbial populations. Thereby, a specific microbial biofilm is able to colonize plastic debris in marine environments [31, 32]. These microbial communities can contain potential harmful species [31, 33] and vary in their structure and composition depending on geographic position, season, and polymer type [34].

Although the occurrence of microplastics in aquatic ecosystems is well-documented and potential risks for the aquatic biota are indicated, a valid and standardized analytical system to identify and quantify microplastics in environmental samples is still missing [2]. Studies reporting the presence of microplastics in environmental systems are only partially comparable because of the variety of methods regarding sampling, preparation, identification, and size classification [2]. Investigation of microplastic samples by visual methods alone can lead to misidentification and, depending on the size of the particles, to over- or underestimation [2, 35]. A trustworthy identification of microscopic particles includes two consecutive steps: first, the decision whether a particular particle is a synthetic polymer or not and second, the identification of its polymer type. Both are solely possible on the basis of their chemical structure. For this purpose, sequential pyrolysis-gas chromatography coupled to mass spectrometry (py-GC/MS) [8] and vibrational spectroscopic methods like Fourier transform infrared

(FTIR) spectroscopy [3, 4] or Raman spectroscopy [10, 13] are usually used. The advantage of py-GC/MS is the detection of both polymer type of a microplastic particle and contained plastic additives simultaneously [36]. However, this approach works only for isolated particles after a visual presorting and is size limited by the ability of handling particles manually [36]. A further disadvantage of py-GC/MS is the destruction of the investigated particles during the analysis.

To overcome the aforementioned limitations, the use of a non-invasive characterization method is highly recommended. If coupled with a microscope, spectroscopic methods (Raman or FTIR) provide chemical structure information combined with high lateral resolution. In the case of Raman microscopy, a lateral resolution up to 500 nm can be achieved with a 532-nm laser and a $\times 100$ objective (NA=0.75). Hence, Raman imaging offers the potential of an automatable method to analyze microplastics directly on filters without any visual presorting, furthermore, to investigate large filter areas. However, it is necessary to eliminate disturbing biological components by an efficient sample preparation to avoid fluorescence during the Raman measurement. Otherwise, fluorescence due to the presence of a biofilm superposes the Raman signal, which can fully hamper particle identification. Furthermore, an automated process ensuring optimal focusing on each potential microplastic particle is needed. These are current challenges to cope with.

The second promising non-invasive technique in this field is FTIR microscopy and FTIR imaging. Recently, Loder et al. suggested an analysis protocol for the identification of microplastics in environmental samples using focal plane array detector (FPA)-based FTIR imaging. After sample extraction via density separation [37] and enzymatic purification, the complete environmental sample (e.g., plankton or sediment) is concentrated on a filter [35]. Subsequently, the whole filter area (about 10 mm in diameter) is measured automatically without any visual presorting and is analyzed via FTIR imaging [35]. This optimized analytical approach allows the detection of microplastics with a particle size down to 20 μm during a semi-automated process [35]. To do this, FTIR imaging has to be performed in transmission mode. Specular reflection FTIR imaging does not give satisfying results because polymer surfaces in principle reflect IR radiation very weakly and irregular-shaped particles cause refractive error resulting from the superposition of directed and undirected reflection [35, 38]. The attenuated total reflection (ATR) technique combined with a FTIR microscope is suitable for the investigation of large microplastic particles ($>500 \mu\text{m}$) [12, 35]. However, an automatable mapping or imaging method in ATR mode is not realizable for small microplastics due to the risk that particles adhere to the ATR crystal during the measurement and, furthermore, it is extremely time-consuming.

For transmission FTIR imaging of microplastic samples concentrated on filters, a suitable filter substrate is crucial.

For this purpose, the filter substrate has to be IR transparent at a wide spectral range (no self-absorption) for distinct polymer identification. In addition, it has to be water-resistant and mechanically stable and it must include pores or holes to enable vacuum filtration of aqueous samples. Conventional IR transparent substrates are either water-soluble (NaCl, KBr, and CsI), toxic (KRS-5—a solid solution of thallium bromide and thallium iodide) or they are not suitable for creating holes or pores (CaF₂, ZnS, etc.) [39]. Löder et al. tested different commercially available filter substrates and recommended an aluminum oxide membrane filter (Anodisc, Whatman) for transmission FTIR imaging of environmental microplastic samples. However, this filter material is usable only in a limited spectral range from 3800 to 1250 cm⁻¹ [35]. Due to the self-absorption of the Anodisc filter in the mid-infrared fingerprint range (1400–600 cm⁻¹), a distinct identification of potential microplastic particles and an accurate classification of the polymer type is strongly restricted or even not possible in every case. Moreover, the aluminum oxide filter shows a relative high fragility, which hampers excessive handling.

Our work suggests and describes a novel silicon (Si) filter substrate for FTIR imaging of environmental microplastic samples produced by photolithographic microstructuring. This filter type fulfills all requirements mentioned, in particular it guarantees good transparency for the broad mid-infrared region of 4000–600 cm⁻¹, features holes with a diameter of 10 μm, and exhibits adequate mechanical stability. Furthermore, it will be shown that this novel Si filter substrate is able to be applied for transmission FTIR microscopy and imaging as well as for Raman microscopy of microplastic samples.

Methodology

Fabrication of the Si filter substrate

To prepare a conventional Si wafer for filtering purposes, through holes were generated in the wafer by semiconductor fabrication techniques. The manufacturing of our Si filter substrates involves the following basic technology steps:

1. Etch mask formation by photolithography
2. Blind via formation by deep reactive ion etching (DRIE)
3. Through hole formation by bulk silicon thinning using mechanical grinding/polishing technology
4. Separation of the thinned silicon filter substrates by stealth dicing

This process allows the manufacturing of Si filter substrates at low costs on 300-mm silicon wafers with standard wafer-level production equipment used in the semiconductor industry. The schematic process flow is shown in Fig. 1.

In detail, a standard 300-mm boron-doped silicon wafer was used, characterized by the following properties: resistivity range 14–21 Ω cm, orientation <100>, thickness ~775 μm. First, a positive tone photoresist layer (AZ9260) was spin coated on the silicon wafer until reaching a layer thickness of ~17 μm. The layer was structured by a 1× mask aligner lithography using a 14" soda-lime glass/chrome mask. Second, blind holes were etched into the bulk silicon using an inductively coupled plasma source reactor applying a modified Bosch process. Sulfur hexafluoride (SF₆) and octafluorocyclobutane (C₄F₈) were used as etch gasses. The etch depth was adjusted to >255 μm to ensure enough etch depth for the final through hole-opening process. Details of the deep silicon etching mechanism are described elsewhere [40–43]. Third, the substrate was mounted on a film frame carrier with the wafer top side face down to allow wafer thinning and polishing to a target thickness of 245–250 μm. This process step opens the through holes from the wafer back side mechanically. Finally, the thinned silicon wafer was singularized into quadratic filters using stealth dicing technology [44].

To characterize the obtained Si filter substrate, microscopic and scanning electron microscopic (SEM) images were recorded with an Eclipse L300N microscope (Nikon) combined with a ConfoCam C101 confocal head (Confovis) and with a LEO 1530 scanning electron microscope (Zeiss) at 10 kV accelerating voltage, respectively. The samples were sputter coated with Au/PD prior to SEM analysis.

Construction of the filter adapter

To make the quadratic Si filter substrates useable as filters together with conventional filter holders and in order to reduce the filtering area for the subsequent FTIR imaging [35], a special filter adapter was developed. For this purpose, a silicone seal was poured into a supporting ring of polymethyl methacrylate (PMMA), molding its top and bottom by two additional parts of PMMA. The two-component silicone (Elastosil RT 625, Wacker) was mixed in vacuum to reach an optimal degassing. All PMMA parts were CNC milled.

Microplastic model samples

Microplastic model samples were produced as thin melt films (15 μm) of commercial pellets of high-density polyethylene (HDPE), polypropylene (PP), polyethylene terephthalate (PET), and polybutylene terephthalate (PBT) with a heated press (Specac). For the melting process, temperatures of 140 °C (HDPE), 165 °C (PP), 265 °C (PET), and 240 °C (PBT) and a pressure of 3 tons were used. The polymer films were cut into small pieces of about 1×2 mm² for FTIR and Raman single measurement and of about 0.5×0.5 mm² for FTIR imaging respectively.

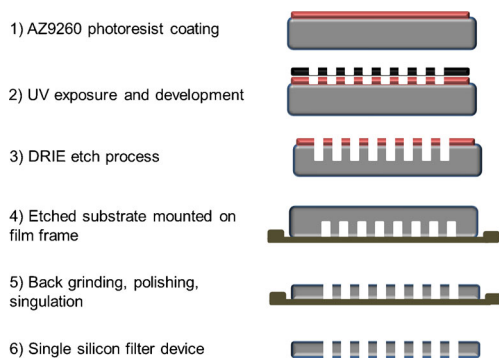


Fig. 1 Schematic process flow to manufacture Si filter substrates on wafer-level production equipment

Spectroscopic measurements

FTIR microscopy and FTIR imaging

FTIR microscopy Single measurements were performed with a Vertex 70 spectrometer (Bruker) coupled with a Hyperion 2000 FTIR microscope (Bruker) with a $\times 15$ IR objective and a Mercury Cadmium Telluride (MCT) single element detector. Small pieces ($\sim 1 \times 2 \text{ mm}^2$) of the polymer films were placed separately onto the Si filter substrate and onto the Anodisc filter, respectively. The FTIR spectra of every particle were recorded consecutively in transmission mode in a wavenumber range of $4000\text{--}600 \text{ cm}^{-1}$ with a spectral resolution of 4 cm^{-1} . Thirty-two scans were co-added for every spectrum, and zero-filling factor 4, Blackmann-Harris three-term apodization, and Mertz phase correction were used. The background was measured with the same settings against air or against the investigated substrate.

FTIR imaging Measurements were carried out using a Tensor 27 FTIR spectrometer (Bruker) coupled with a Hyperion 3000 FTIR microscope (Bruker) with a $\times 15$ IR objective and a 64×64 FPA detector. The simultaneous measurement of all small polymer films ($\sim 0.5 \times 0.5 \text{ mm}^2$) placed on the Si filter substrate was performed in transmission mode in a wavenumber range of $4000\text{--}900 \text{ cm}^{-1}$ using a spectral resolution of 8 cm^{-1} . FPA fields, 6×9 , covering an area of $1000 \times 1500 \text{ }\mu\text{m}^2$ were measured. Sixteen scans were co-added for every spectrum, and zero-filling factor 2, Blackmann-Harris three-term apodization, and Mertz phase correction were chosen. The background was measured with the same parameters but apart from that with 32 co-added scans against the Si filter substrate without any sample.

Both FTIR instruments were controlled by OPUS 7.5 software (Bruker). All FTIR spectra shown in this study were smoothed (Savitzky-Golay, 13 points) for better illustration.

Raman microscopy

Raman spectra were recorded by the confocal Raman microscope and imaging system alpha 300R (WITec), equipped with a 532-nm laser and a thermoelectrically cooled charge-coupled device (CCD) detector. The measurements were performed with a $\times 20$ objective and a laser power of 10 mW. The integration time was 500 ms, and 100 scans were accumulated. The Raman system was operated by Control FOUR plus software (WITec).

Results and discussion

Characterization of the Si filter substrate

The Si filter substrate covers an area of $11 \times 11 \text{ mm}^2$ and contains through holes with a nominal diameter of $10 \text{ }\mu\text{m}$ and a pitch of $55 \text{ }\mu\text{m}$. It offers a hole density of approximately 380 holes/mm^2 . Details of the filter design are shown in Fig. 2. A main part of $22 \times 22 \text{ mm}^2$ is repeated on a 300-mm silicon wafer, and subsequently four Si filter substrates ($11 \times 11 \text{ mm}^2$) are singularized out of each. Thus, 540 single filters ($11 \times 11 \text{ mm}^2$) can be obtained from one 300-mm silicon wafer. The technology allows to adjust pitch and diameter of the holes easily and to change final Si filter substrate geometry to fit specific geometric requirements.

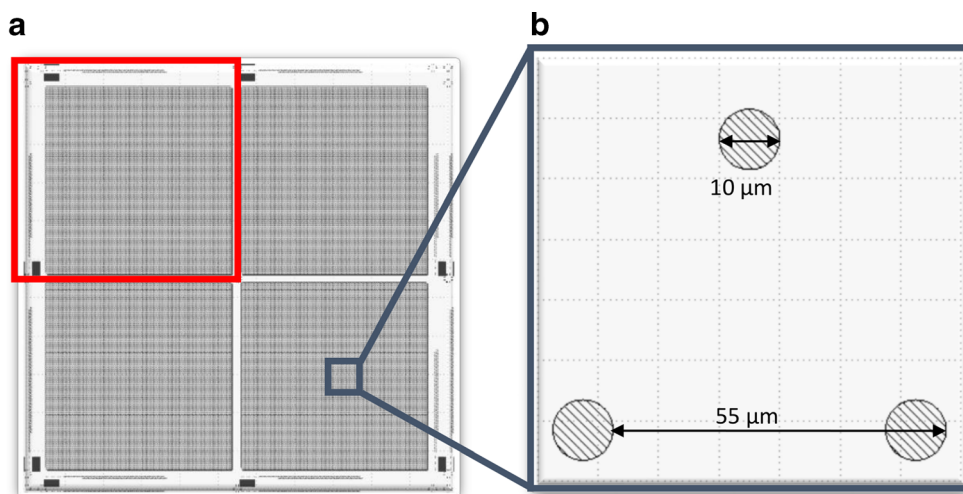
Microscope images of the obtained Si filter substrate compared with the Anodisc filter are shown in Fig. 3. Due to the technology, the hole diameter ranges from $16 \text{ }\mu\text{m}$ on the top side to approximately $10 \text{ }\mu\text{m}$ on the Si filter back side. During Bosch process, the AZ9260 photoresist is consumed, which weakens protection of the upper hole areas. Hence, a widening of the hole diameter on the top side occurs compared to the dimension obtained after photoresist development. However, since the Si filter is usable on both sides, the enlarged hole diameter on the top side does not pose a problem. Compared with the Si filter substrate, the Anodisc filter does not show a defined structure, in fact irregular pores can be observed.

A SEM image of a hole cross section of the Si filter substrate is shown in Fig. 4. A conical etch profile can be clearly seen. In the deeper regions of the through hole (etch depth $> 150 \text{ }\mu\text{m}$), grooves in the silicon sidewall are observed, which are caused by the used Bosch process parameters. The sidewall profile can be further optimized, if needed for the application.

To characterize the spectroscopic properties of the obtained Si filter substrate, transmission FTIR microscopy single measurements compared with the conventional Anodisc filter were performed. The resulting spectra are shown in Fig. 5.

The Anodisc filter shows very strong self-absorption from 1250 down to 600 cm^{-1} , in addition to a medium intensive absorption doublet in the range of $1745\text{--}1375 \text{ cm}^{-1}$.

Fig. 2 Design of the Si filter substrate. (a) Main part ($22 \times 22 \text{ mm}^2$) including four Si filter substrates of $11 \times 11 \text{ mm}^2$ (red square). (b) Details of the hole design ($10 \mu\text{m}$ diameter, $55 \mu\text{m}$ pitch)



According to Löder et al., the Anodisc filter is consequently usable as substrate for transmission FTIR measurements only in the spectral range of $4000\text{--}1250 \text{ cm}^{-1}$. Especially, the fingerprint region ($1400\text{--}600 \text{ cm}^{-1}$) including characteristic bands for distinct polymer identification is strongly restricted.

In contrast, the Si filter substrate does not show any intensive absorption bands in the mid-IR region from 4000 to 600 cm^{-1} . Only weak peaks at 1108 , 883 , and 741 cm^{-1} can be observed (inlet spectrum in Fig. 5). The band at 1108 cm^{-1} results from asymmetric Si-O-Si stretching vibrations caused by interstitial oxygen impurity in the silicon lattice [45, 46]. The other two bands are attributed to different lattice vibrations in silicon (phonon absorption). Furthermore, an absorption band at the high-wavelength edge of the spectrum at about 610 cm^{-1} can be observed. This band results from a combination of phonon absorption and of Si-C vibrations caused by substitutional carbon impurity [46].

The mentioned absorption bands of the Si filter substrate show very weak intensity compared to the bands of the Anodisc filter. In a previous study on FTIR imaging of

microplastics [35], a maximum acceptable absorbance value of 0.5 for self-absorption by the filter material was discussed to ensure the detection of weak bands of microplastic particles. This requirement is highly fulfilled by our novel Si filter substrate in the whole range of $4000\text{--}600 \text{ cm}^{-1}$.

Of course, the transmission spectrum of pure Si filter substrates show spectral interferences due to multiple reflections of the IR beam between the two plane-parallel boundary surfaces of the Si filter substrate. The intensity of the interference pattern depends on the thickness of the substrate and decreases with increasing thickness. A Si filter substrate with a thickness of $250 \mu\text{m}$ has been proved to be suitable in preliminary tests. Using the pure substrate as background, this effect was eliminated in the spectra of the microplastics.

Our filter adapter, which facilitates filtering of aqueous microplastics samples using the novel Si filter substrate, is shown in Fig. 6. The conical-shaped silicone seal narrows its inner diameter from 13 mm at the top side to 9 mm at the filtration outfall. Thus, the filtration area is reduced what is important to limit measurement time and amount of data for the subsequent FTIR imaging [35]. An additional feature of

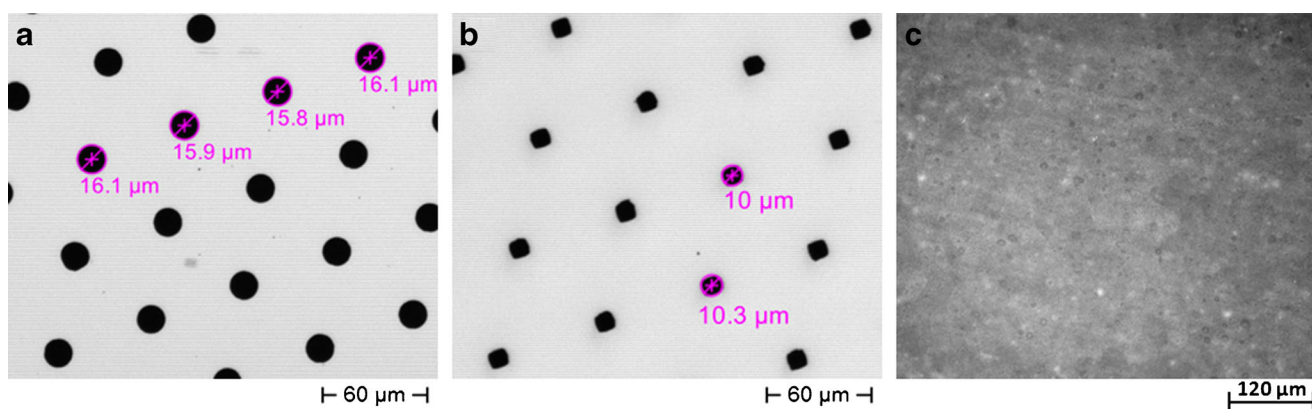
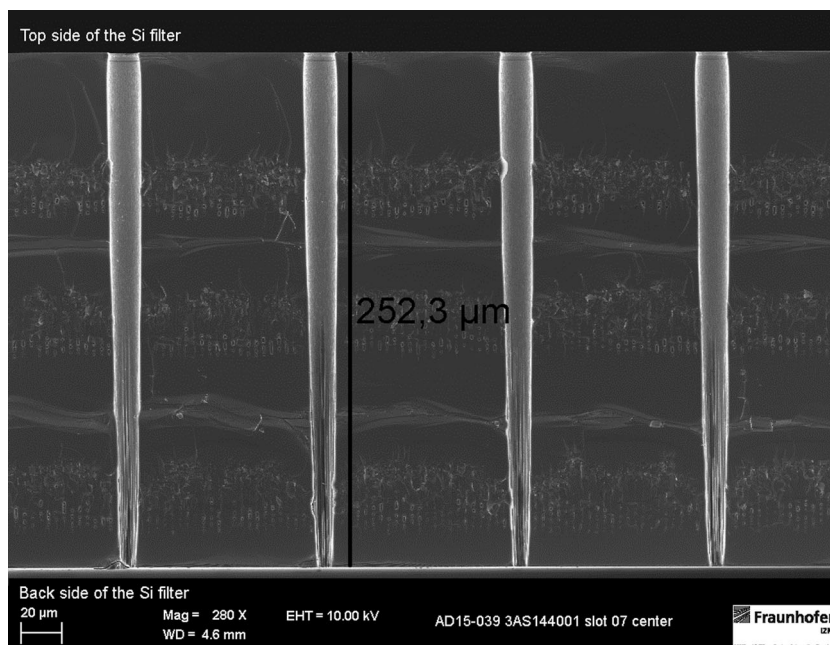


Fig. 3 Light microscopic images. (a) Top side of the Si filter substrate. (b) Back side of the Si filter substrate. (c) Anodisc filter (darkfield modus)

Fig. 4 SEM image of the cross section of silicon filter through holes



the silicone seal is a quadratic cutout with an area of $11 \times 11 \text{ mm}^2$ and a depth of 0.2 mm (Fig. 6) to avoid displacement of the Si filter substrate during filtration and to guarantee water tightness.

The filter adapter can be used in a combination with a commercial available microanalysis filter holder (Merck) consisting of a removable glass funnel, a glass base with integrated glass frit, a silicone stopper, and a metal clip (Fig. 6). We used a custom glass funnel with an inner diameter of 13 mm in contrast to the original one with an inner diameter of 17 mm. Filtration was carried out by a conventional filtering flask coupled with a vacuum pump (e.g., water-jet). The Si filter was placed into the filter adapter with the top side face down.

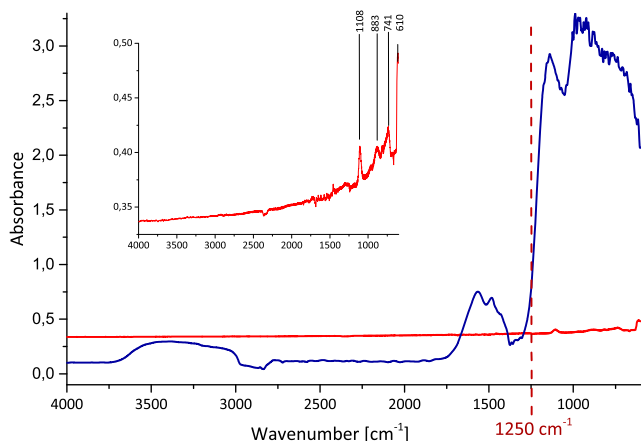


Fig. 5 FTIR transmission spectra of the novel Si filter substrate (red) and the conventional Anodisc filter (blue). The inset spectrum shows absorption properties of the Si filter substrate (thickness, 250 μm) in detail

FTIR spectroscopic identification of microplastic model samples: comparison of Si and Anodisc filters

FTIR microscopy

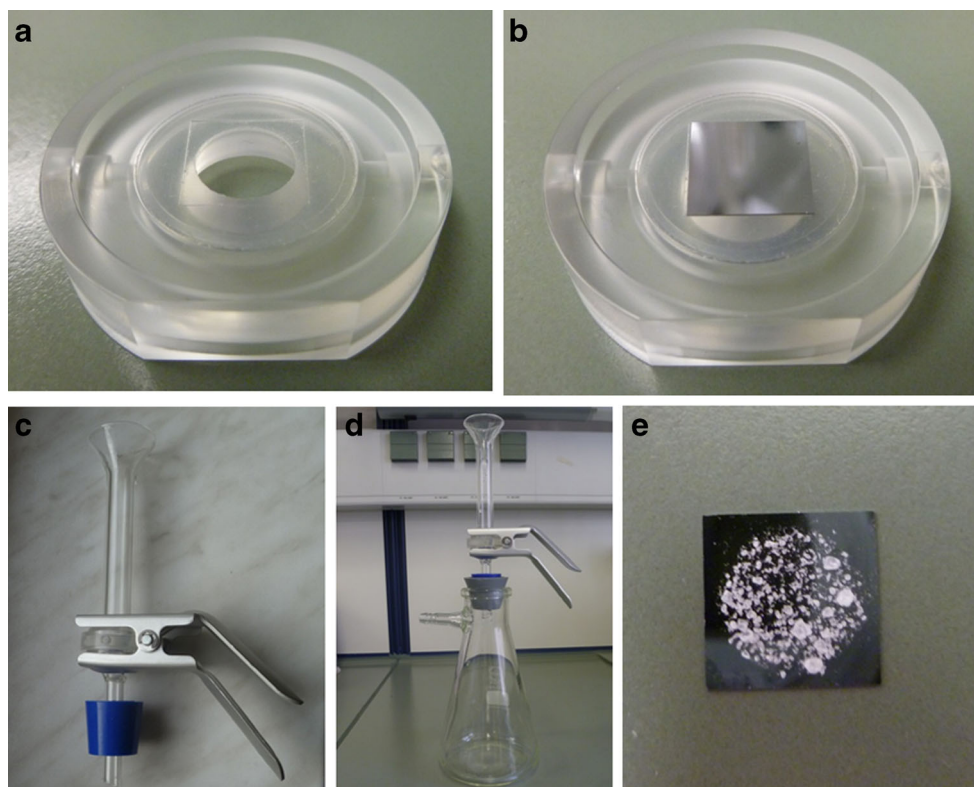
First, the applicability of the Si filter substrate to identify different microplastic models was tested by single transmission FTIR microscopy measurements. For this purpose, small pieces of thin films of PE and PP—the most common synthetic polymers identified so far in microplastic samples [2]—were investigated. The results are shown in Fig. 7.

In the range of $3000\text{--}2800 \text{ cm}^{-1}$, CH_2 (PE) and CH_2/CH_3 (PP) stretching vibration bands are clearly seen in the spectra regardless of the filter substrate. Although the investigated microplastic model films are relatively thin ($15 \mu\text{m}$) compared with the thickness expected for real environmental microplastic particles, total absorption appears in this spectral range. Thus, a further characterization of these bands is not possible and their analytical worth is limited.

The bending vibration of the CH_2 and CH_3 groups can be observed in the range of $1500\text{--}1350 \text{ cm}^{-1}$. However, the self-absorption band of the Anodisc filter (blue) superposes the band at approx. 1460 cm^{-1} of both PE and PP. In contrast, the Si filter substrate (orange) does not influence the polymer spectra in this spectral range.

Due to the very strong self-absorption of the Anodisc filter from 1250 to 600 cm^{-1} , polymer bands in this range are completely masked. The Si filter substrate opens this region and allows the detection of vibration bands in the fingerprint region and below. Therefore, CH_2 rocking vibration at 725 cm^{-1} can be observed in the PE spectrum and numerous bands between 700 and 1200 cm^{-1} caused by coupling of CH_3

Fig. 6 Photos of the filter adapter and the complete filter unit. **(a)** Bottom of the filter adapter, quadratic cutout in the silicone seal is shown. **(b)** Filter adapter with inserted Si filter substrate. **(c)** Microanalysis filter holder (Merck) with integrated filter adapter. **(d)** Filter holder mounted on a vacuum filtering flask. **(e)** Si filter substrate after filtration of a microplastic model sample of fragmented particles of PE and polystyrene



and CH_2 rocking and C-C stretching vibrations [47] in the PP spectrum become visible.

In the “operating range” of the Anodisc filter (4000 to 1250 cm^{-1}), the absorption profiles of the two investigated aliphatic polymers are relatively similar. Hence, a differentiation between PE and PP is solely possible with the

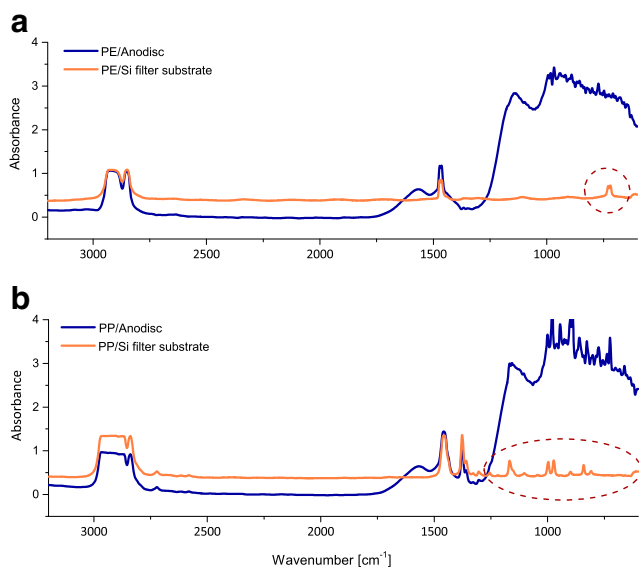


Fig. 7 FTIR transmission spectra of PE **(a)** and PP **(b)** on an Anodisc filter (blue) and on the Si filter substrate (orange) without subtraction of the filter signal (background: air). PE and PP bands which are detected exclusively by applying the Si filter substrate are marked (red circle)

aid of the symmetric CH_3 bending band at 1377 cm^{-1} . On the contrary, the Si filter substrate allows differentiation and identification of the two polymers unambiguously by means of the additional bands in the fingerprint region. Furthermore, the main absorption bands of PE, PP, and other synthetic polymers in the range from 3200 to 1250 cm^{-1} (CH_2 and CH_3 stretching at 3000 – 2800 cm^{-1} and CH_2 and CH_3 bending at 1500 – 1350 cm^{-1}) are not specific enough to recognize potential microplastic particles as synthetic polymers without any doubt because most organic substances (e.g., low-molecular hydrocarbons, technical waxes, etc.) show vibration bands in the same ranges [47]. To identify and to classify environmental microplastic particles, the complete mid-infrared spectrum including the fingerprint region should be examined. As it is shown in Fig. 7, the Si filter substrate ensures better results in comparison with the conventional Anodisc filter for this purpose.

As a second example, PET and PBT microplastic model particles were investigated on the two filter substrates. PET and PBT are both thermoplastic polyesters; however, PET is used in high amounts, e.g., in food packaging (bottles, foils, etc.) and in textiles [47], whereas PBT is processed in special applications for, e.g., electrical engineering or automobile industry [48]. The chemical structure of PET and PBT differs only in the length of the aliphatic segment within the monomeric unit. Therefore, the FTIR spectra of both polymers are quite similar (Fig. 8).

Fig. 8 FTIR transmission spectra of PBT (blue) and PET (green) on the Anodisc filter (a) and on the Si filter substrate (b) after subtraction of the corresponding background (Si filter substrate or Anodisc filter, respectively)

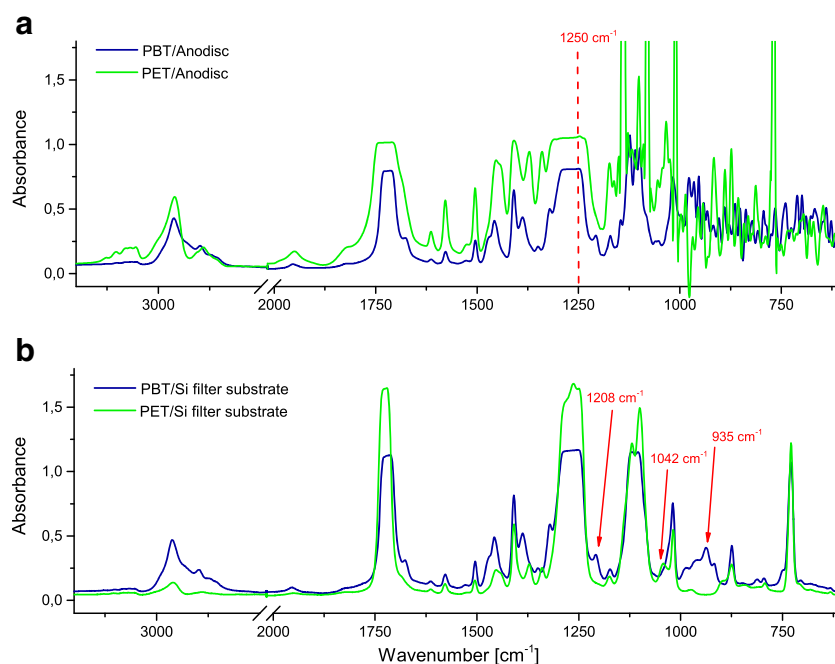


Figure 8a shows a comparison between PET und PBT on the Anodisc filter. The very strong self-absorption of the Anodisc from 1250 to 600 cm^{-1} does not permit signal evaluation in this spectral range. Vibration bands of samples placed on the Anodisc filter are completely overlapped in this spectral region. PET and PBT show nearly identical absorption profiles in the fore spectral range (3200–1250 cm^{-1}), which makes it impossible to differentiate both polymers.

Figure 8b displays the comparison of PET and PBT spectra measured using the Si filter substrate. Contrary to the Anodisc filter, all characteristic bands of the polymers are visible. A detailed examination of the bands in the range between 1500 and 600 cm^{-1} allows recognizing differences between PET and PBT. For example, PBT shows additional bands at 1208 and

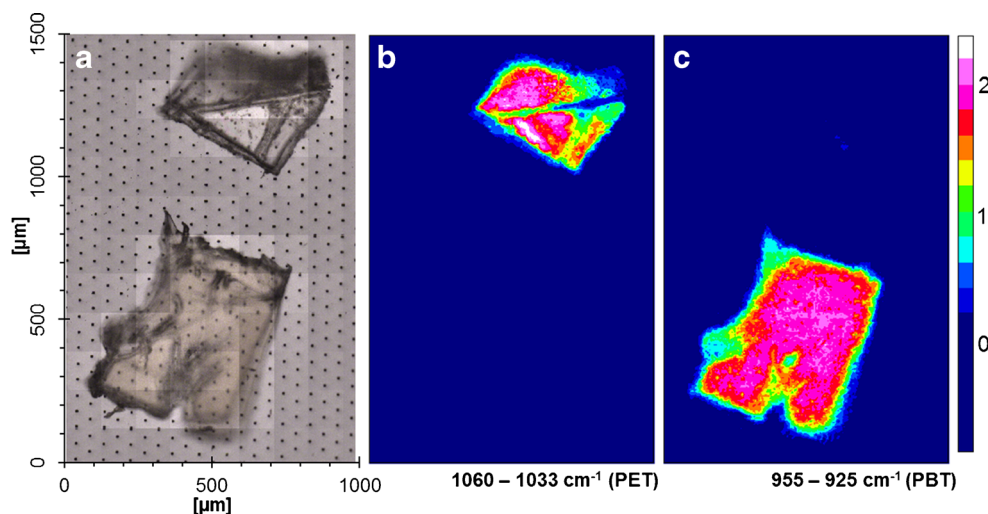
935 cm^{-1} , which are not be found in PET. Moreover, in the PET spectrum, a characteristic band at 1042 cm^{-1} —not existing in PBT—can be observed. This band at 1042 cm^{-1} can be described as a structure and orientation sensitive band of the ethylene glycol linkage in the gauche form within PET [49]. The band at 935 cm^{-1} is related to the amorphous phase of PBT [50].

With the help of the characteristic absorption profiles in the range from 1500 to 600 cm^{-1} , a distinct differentiation between PET and PBT by using the Si filter substrate is possible.

FTIR imaging

These mentioned bands of PET (1042 cm^{-1}) and PBT (935 cm^{-1}) can be used to generate respective FTIR images.

Fig. 9 Optical image (“video image”) (a) and FTIR images (b+c) of a microplastic model sample of PET and PBT. The FTIR images were generated by choosing the band region of 1060–1033 cm^{-1} for PET (b) or of 955–925 cm^{-1} for PBT (c) for integration. The color scale represents the intensity of an integrated band. All pictures have the same lateral dimensions as labeled at the optical image



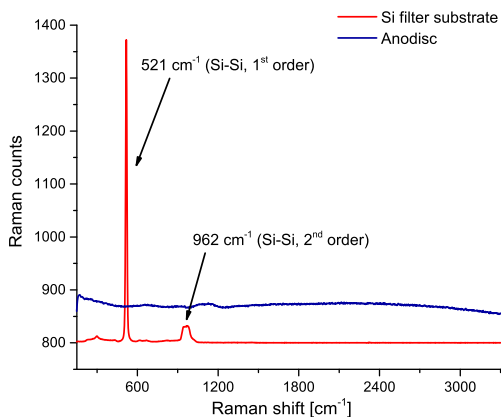
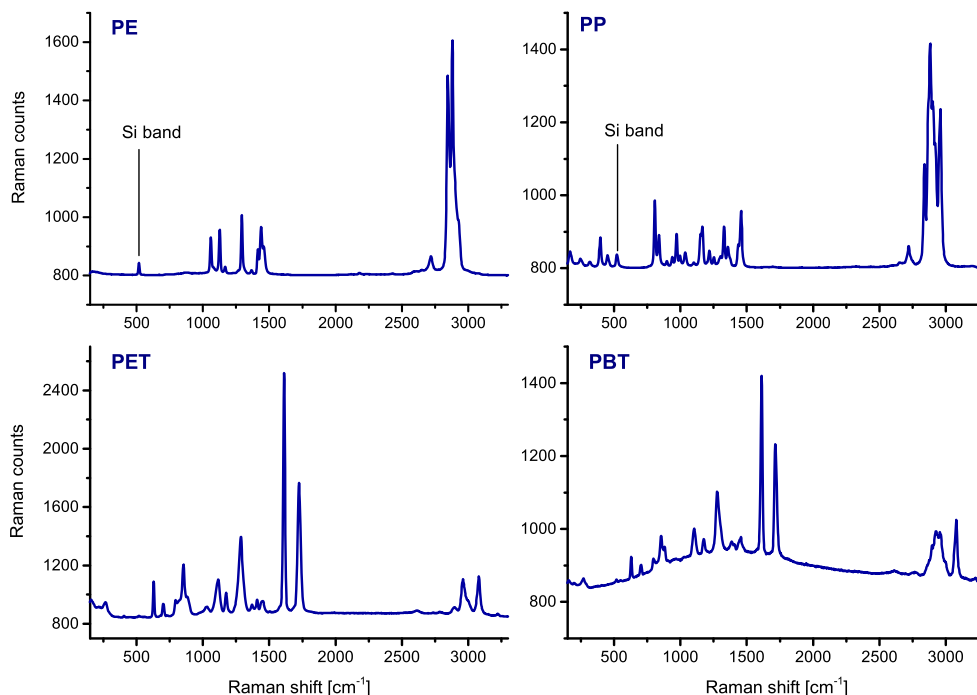


Fig. 10 Raman spectra of the Anodisc filter (blue) and the Si filter substrate (red)

Figure 9 shows the optical image (left) of a microplastic model sample, consisting of small pieces ($0.5 \times 0.5 \text{ mm}^2$) of PET and PBT films ($15 \text{ }\mu\text{m}$), as well as the corresponding FTIR images recorded using the FPA detector. To illustrate the microplastic particles, the spectral range of $1060\text{--}1033 \text{ cm}^{-1}$ (PET) and $955\text{--}925 \text{ cm}^{-1}$ (PBT), respectively, was chosen. Regions of the sample area with a high intensity of the chosen integrated absorption band are colored red.

As seen in Fig. 9, FTIR imaging of microplastic samples on the novel Si filter substrate can be performed and analyzed successfully. Furthermore, it is even possible to show the distribution of two quite similar polymers as PET and PBT within a microplastic sample. By choosing characteristic and appropriate bands, the FTIR imaging works excellently for the discrimination of other synthetic polymers, too.

Fig. 11 Raman spectra of four different microplastic models (pieces of thin films) of PE, PP, PET, and PBT located on the Si filter substrate



Raman microscopy of microplastic model samples on Si filter substrate

Additionally, our Si filter was tested as a substrate for Raman microscopy, the second promising non-invasive method to detect microplastic samples. The aim is to have a substrate which can be applied for the analysis of microplastics via both FTIR and Raman spectroscopy.

Using Raman spectroscopy, scattering of monochromatic light illuminating mainly the surface region (up to several hundred microns) of a sample is detected. Therefore, the measurement substrate is not as crucial as with transmission FTIR spectroscopy. However, during the investigation of thin and transparent samples, vibrations of the underlying substrate can be detected. Thus, the filter substrate for Raman microscopy and Raman imaging of microplastic samples should not exhibit any own bands in the range of the polymer bands; furthermore, it optimally should not show any fluorescence.

In Fig. 10, the Raman spectra of the Anodisc filter and the Si filter substrate are illustrated. The first- and second-order Si-Si vibration at 521 and 962 cm^{-1} can clearly be seen in the spectra of the Si filter substrate. In contrast, the Anodisc filter does not show any own vibration bands; however, a weak fluorescence profile can be observed.

To examine whether the Si vibration bands influence the Raman spectra of synthetic polymers, four different microplastic model samples of PE, PP, PET, and PBT were measured exemplarily. The results are shown in Fig. 11.

The Si-Si band at 521 cm^{-1} can be seen in the spectra of PE and PP though it does not interfere with the polymer bands.

All characteristic peaks of these polymers are clearly visible and separated from the Si band. In the spectra of PET and PBT, the Si band cannot be observed. Probably, these investigated polymer films overlay the Si filter substrate completely due to their thickness or opacity.

In summary, the Si filter substrate does not show any fluorescence and its own vibration bands do not disturb the polymer spectra. Therefore, it is a suitable substrate for the detection of microplastic samples by Raman microscopy.

Conclusion

Within this study, we described the technical development of a novel Si filter substrate and demonstrated its advantages for vibrational spectroscopic measurements compared with the conventional Anodisc filter for identification of microplastics. In summary, our Si filter is an appropriated substrate for transmission FTIR microscopy and FTIR imaging as well as for Raman microscopy of microplastic samples. By using a combination of FTIR and Raman, difficulties of one method during microplastics analysis can be overcome by the other method. For example, thick particles often lead to total absorption in the FTIR transmission spectra, so that evaluation of absorption bands and consequent particle identification is hindered or even not possible. In this case, Raman spectroscopy can be a remedy since it is independent of the particle thickness. Secondly, because the lateral resolution of spectroscopic imaging is limited by diffraction (dependent on wavenumber and numerical aperture of the microscope objective), FTIR imaging does not allow detecting particles smaller than 10–20 μm [35]. By using Raman microscopy and imaging, a higher lateral resolution (up to 500 nm) can be achieved and even smaller particles can be identified.

In addition to the spectroscopic benefit, the Si substrate offers good mechanical stability and enables filtration of aqueous samples due to its well-defined holes. Moreover, with the aid of a special developed filter adapter, the practical applicability of the Si filter substrate to filtrate microplastic samples has been demonstrated.

Acknowledgments We thank Vincent K rber (IPF) and the construction team for technical support and Dr. Cordelia Zimmerer (IPF) for helpful discussion regarding FTIR imaging. The authors also would like to thank Rene Puschmann, Michael Lorenz, Tina Klemmt, and Dr. Frank Menzel from Fraunhofer IZM-ASSID for assistance with manufacturing of the Si filter substrate. We are also grateful to Dr. Sonja Oberbeckmann (Leibniz IOW), Dr. Gunnar Gerdtts (AWI, Helgoland), and Prof. Christian Laforsch (University of Bayreuth) for helpful discussion. Finally, we thank the Leibniz Association for financial support of the project “MikrOMIK.”

References

1. Andrady AL (2011) Microplastics in the marine environment. *Mar Pollut Bull* 62:1596–1605
2. Hidalgo-Ruz V, Gutow L, Thompson RC, Thiel M (2012) Microplastics in the marine environment: a review of the methods used for identification and quantification. *Environ Sci Technol* 46:3060–3075
3. Frias JPGL, Otero V, Sobral P (2014) Evidence of microplastics in samples of zooplankton from Portuguese coastal waters. *Mar Environ Res* 95:89–95
4. Song YK, Hong SH, Jang M, Kang J-H, Kwon OY, Han GM, Shim WJ (2014) Large accumulation of micro-sized synthetic polymer particles in the sea surface microlayer. *Environ Sci Technol* 48:9014–9021
5. Carpenter EJ, Anderson SJ, Harvey GR, Miklas HP, Peck BB (1972) Polystyrene spherules in coastal waters. *Science* 178:749–750
6. Lattin GL, Moore CJ, Zellers AF, Moore SL, Weisberg SB (2004) A comparison of neustonic plastic and zooplankton at different depths near the southern California shore. *Mar Pollut Bull* 49:291–294
7. Doyle MJ, Watson W, Bowlin NM, Sheavly SB (2011) Plastic particles in coastal pelagic ecosystems of the northeast Pacific Ocean. *Mar Environ Res* 71:41–52
8. Dekiff JH, Remy D, Klasmeier J, Fries E (2014) Occurrence and spatial distribution of microplastics in sediments from Nordemey. *Environ Pollut* 186:248–256
9. Van Cauwenberghe L, Claessens M, Vandegehuchte MB, Mees J, Janssen CR (2013) Assessment of marine debris on the Belgian Continental Shelf. *Mar Pollut Bull* 73:161–169
10. Van Cauwenberghe L, Vanreusel A, Mees J, Janssen CR (2013) Microplastic pollution in deep-sea sediments. *Environ Pollut* 182:495–499
11. Lechner A, Keckeis H, Lumesberger-Loisl F, Zens B, Krusch R, Tritthart M, Glas M, Schludermann E (2014) The Danube so colourful: a potpourri of plastic litter outnumbers fish larvae in Europe’s second largest river. *Environ Pollut* 188:177–181
12. Zbyszewski M, Corcoran PL (2011) Distribution and degradation of fresh water plastic particles along the beaches of Lake Huron, Canada. *Water Air Soil Pollut* 220:365–372
13. Imhof HK, Ivleva NP, Schmid J, Niessner R, Laforsch C (2013) Contamination of beach sediments of a subalpine lake with microplastic particles. *Curr Biol* 23:R867–R868
14. Free CM, Jensen OP, Mason SA, Eriksen M, Williamson NJ, Boldgiv B (2014) High-levels of microplastic pollution in a large, remote, mountain lake. *Mar Pollut Bull* 85:156–163
15. Rillig MC (2012) Microplastic in terrestrial ecosystems and the soil? *Environ Sci Technol* 46:6453–6454
16. Fendall LS, Sewell MA (2009) Contributing to marine pollution by washing your face: microplastics in facial cleansers. *Mar Pollut Bull* 58:1225–1228
17. Gregory MR (1996) Plastic “scrubbers” in hand cleansers: a further (and minor) source for marine pollution identified. *Mar Pollut Bull* 32:867–871
18. Hintersteiner I, Himmelsbach M, Buchberger WW (2015) Characterization and quantitation of polyolefin microplastics in personal-care products using high-temperature gel-permeation chromatography. *Anal Bioanal Chem* 407:1253–1259
19. Derrai JG (2002) The pollution of the marine environment by plastic debris: a review. *Mar Pollut Bull* 44:842–852
20. Cole M, Lindeque P, Halsband C, Galloway TS (2011) Microplastics as contaminants in the marine environment: a review. *Mar Pollut Bull* 62:2588–2597

21. Jambeck JR, Geyer R, Wilcox C, Siegler TR, Perryman M, Andrady A, Narayan R, Law KL (2015) Plastic waste inputs from land into the ocean. *Science* 347:768–771
22. Ivar do Sul JA, Costa MF (2014) The present and future of microplastic pollution in the marine environment. *Environ Pollut* 185:352–364
23. Setälä O, Fleming-Lehtinen V, Lehtiniemi M (2014) Ingestion and transfer of microplastics in the planktonic food web. *Environ Pollut* 185:77–83
24. Lee K-W, Shim WJ, Kwon OY, Kang J-H (2013) Size-dependent effects of micro polystyrene particles in the marine copepod *Tigriopus japonicus*. *Environ Sci Technol* 47:11278–11283
25. Van Cauwenberghe L, Janssen CR (2014) Microplastics in bivalves cultured for human consumption. *Environ Pollut* 193:65–70
26. Lusher AL, McHugh M, Thompson RC (2013) Occurrence of microplastics in the gastrointestinal tract of pelagic and demersal fish from the English Channel. *Mar Pollut Bull* 67:94–99
27. Foekema EM, De Groot C, Mergia MT, van Franeker JA, Murk AJ, Koelmans AA (2013) Plastic in north sea fish. *Environ Sci Technol* 47:8818–8824
28. Wright SL, Thompson RC, Galloway TS (2013) The physical impacts of microplastics on marine organisms: a review. *Environ Pollut* 178:483–492
29. Rios LM, Jones PR, Moore C, Narayan UV (2010) Quantitation of persistent organic pollutants adsorbed on plastic debris from the Northern Pacific Gyre's "eastern garbage patch". *J Environ Monit* 12:2226–2236
30. Endo S, Takizawa R, Okuda K, Takada H, Chiba K, Kanehiro H, Ogi H, Yamashita R, Date T (2005) Concentration of polychlorinated biphenyls (PCBs) in beached resin pellets: variability among individual particles and regional differences. *Mar Pollut Bull* 50:1103–1114
31. Zettler ER, Mincer TJ, Amaral-Zettler LA (2013) Life in the "plastisphere": microbial communities on plastic marine debris. *Environ Sci Technol* 47:7137–7146
32. Harrison JP, Schratzberger M, Sapp M, Osborn AM (2014) Rapid bacterial colonization of low-density polyethylene microplastics in coastal sediment microcosms. *BMC Microbiol* 14:232
33. Masó M, Garcés E, Pagès F, Camp J (2003) Drifting plastic debris as a potential vector for dispersing harmful algal bloom ((HAB)) species. *Sci Mar* 67:107–111
34. Oberbeckmann S, Loeder MGJ, Gerds G, Mark Osborn A (2014) Spatial and seasonal variation in diversity and structure of microbial biofilms on marine plastics in northern European waters. *FEMS Microbiol Ecol* 90:478–492
35. Löder MGJ, Kuczera M, Mintenig S, Lorenz C, Gerds G (2015) FPA-based micro-FTIR imaging for the analysis of microplastics in environmental samples. *Environ Chem*. doi:10.1071/EN14205
36. Fries E, Dekiff JH, Willmeyer J, Nuelle M-T, Ebert M, Remy D (2013) Identification of polymer types and additives in marine microplastic particles using pyrolysis-GC/MS and scanning electron microscopy. *Environ Sci Process Impacts* 15:1949–1956
37. Imhof HK, Schmid J, Niessner R, Ivleva NP, Laforsch C (2012) A novel, highly efficient method for the separation and quantification of plastic particles in sediments of aquatic. *Limnol Oceanogr Methods* 10:524–537
38. Harrison JP, Ojeda JJ, Romero-González ME (2012) The applicability of reflectance micro-Fourier-transform infrared spectroscopy for the detection of synthetic microplastics in marine sediments. *Sci Total Environ* 416:455–463
39. Günzler H, Heise HM (1996) IR-Spektroskopie: Eine Einführung. VCH, Weinheim
40. Laermer F, Schilp A (1996) U.S. Patent 5501893, 26.03.1996: method of anisotropically etching silicon
41. Jansen H, de Boer M, Otter B, Elwenspoek M (1995) The black silicon method IV: the fabrication of three-dimensional structures in silicon with high aspect ratios for scanning probe microscopy and other applications. *Proc Micro Electromech Syst*. doi:10.1109/MEMSYS.1995.472548
42. Jansen H, de Boer M, Elwenspoek M (1996) The black silicon method VI: high aspect ratio trench etching for MEMS applications. *Proc Ninth Int Work Micro Electromech Syst*. doi:10.1109/MEMSYS.1996.493989
43. Kenoyer L, Oxford R, Moll A (2003) Optimization of Bosch etch process for through wafer interconnects. *Proc. 15th Bienn Univ Microelectron Symp* :338–339
44. Kumagai M, Uchiyama N, Ohmura E, Sugiura R, Atsumi K, Fukumitsu K (2007) Advanced dicing technology for semiconductor wafer—stealth dicing. *IEEE Trans Semicond Manuf* 20:259–265
45. Krcho D (1997) FTIR spectroscopy for silicon solar cell characterisation. *Proc Aust New Zeal Sol Energy Soc Solar 1997*, pp. 117/1-117/7, presented at ANZSES Solar '97: Sustainable Energy, Canberra, Australian National University, 1 - 3 December 1997
46. Vidrine DW (1980) Room temperature carbon and oxygen determination in single-crystal silicon. *Anal Chem* 52:92–96
47. Hummel DO, Scholl F (1988) Atlas der Polymer- und Kunststoffanalyse, Band 2 Kunststoff, Fasern, Kautschuk, Harze, Ausgangs- und Hilfsstoffe, Abbauprodukte - Teil b/I. VCH, Weinheim
48. Olabisi O (1997) Handbook of thermoplastics. Marcel Dekker, New York
49. Schmidt PG (1963) Polyethylene terephthalate structural studies. *J Polym Sci* 1:1271–1292
50. Menzheres GY, Moysa EG, Miks R (1984) IR spectra and structure of polybutylene terephthalate. *Theor Exp Chem* 20:222–226